



JAAS

Comparison of machine learning techniques to optimize the analysis of plutonium surrogate material via a portable LIBS device

Journal:	<i>Journal of Analytical Atomic Spectrometry</i>
Manuscript ID	JA-ART-10-2020-000435.R1
Article Type:	Paper
Date Submitted by the Author:	13-Nov-2020
Complete List of Authors:	Rao, Ashwin; Air Force Institute of Technology Jenkins, Phillip; Air Force Institute of Technology Auxier, John; Los Alamos National Laboratory, Actinide Analytical Chemistry Shattan, Michael; Air Force Institute of Technology

SCHOLARONE™
Manuscripts

Journal Name

ARTICLE TYPE

Cite this: DOI: 00.0000/xxxxxxxxxx

Comparison of machine learning techniques to optimize the analysis of plutonium surrogate material via a portable LIBS device

Ashwin P. Rao,^a Phillip R. Jenkins,^a John D. Auxier II,^b and Michael B. Shattan^{*a}

Received Date
Accepted Date

DOI: 00.0000/xxxxxxxxxx

The utilization of machine learning techniques has become commonplace in the analysis of optical emission spectra. These methods are often limited to variants of principal components analysis (PCA), partial-least squares (PLS), and artificial neural networks (ANNs). A plethora of other techniques exist and are well established in the world of data science, yet are seldom investigated for their use in spectroscopic problems. In this study, machine learning techniques were used to analyze optical emission spectra of laser-induced plasma from ceria pellets doped with silicon in order to predict silicon content. A boosted regression ensemble model was created, and its predictive accuracy was compared to that of traditional PCA, PLS, and ANN regression models. Boosted regression tree ensembles yielded fits with R-squared (R^2) values as high as 0.964 and mean-squared errors of prediction ($MSEPs$) as low as 0.074, providing the most accurate predictive model. Neural networks performed with slightly lower R^2 values and higher $MSEPs$ compared to the ensemble methods, thus indicating susceptibility to overfitting.

1 Introduction

Laser-induced breakdown spectroscopy (LIBS) is a versatile technique for spectroscopic analysis.^{1–3} Modern LIBS experiments are often coupled with advanced mathematical and statistical methods to provide chemical analysis of LIBS spectra, known as chemometrics.^{4–7} Due to the complex nature of the spectra of heavier elements, LIBS data sets for classification and regression problems can contain tens of thousands of emission variables to process. The complexity of these data sets has garnered interest in applying machine learning algorithms to these spectroscopic analysis problems. Techniques such as principal components analysis (PCA) and partial-least squares (PLS) are often used in LIBS analysis to reduce dimensionality of the data and provide accurate classification or regression models.⁸ Recently, these methods have demonstrated their use in a variety of fields, such as food science,⁹ pharmaceutical chemistry,¹⁰ nuclear forensics,¹¹ metallurgy,¹² and analysis of Martian geological samples.^{13,14} Advanced machine learning algorithms based on neural network architectures are commonly used to handle large spectral data sets and provide improved classification or regression solutions.¹⁵ Artificial neural networks (ANNs) have demonstrated significant use in geological and metallurgical applications, creating predictive chemical analysis models from complex spectra of rock,^{16,17}

soil,^{18,19} and ore²⁰ samples.

Portable LIBS (pLIBS) systems have garnered great interest for rapid, *in-situ* chemical analysis.²¹ Devices such as the SciAps Z series were originally built for identifying industrial metals in manufacturing and scrapping industries.²² However, these devices have been used experimentally for geochemical analysis,^{23,24} industrial hygiene,²⁵ landmine detection,²⁶ and detection of rare earth metals.²⁷ Recently, the Z series devices have demonstrated use in nuclear applications, including detection of uranyl fluoride contamination²⁸ and quantitative chemical analysis of plutonium and plutonium surrogates.^{29–31} While these devices enable rapid spectral acquisition with little-to-no sample preparation, their fixed signal integration periods, limited spectral resolutions, and non-linear spectral response yield complicated sets of emission data. This highlights the need to couple these devices with machine learning techniques, especially when analyzing the complex optical emission spectra of lanthanides and actinides used in nuclear applications.

One particular nuclear application where these devices are of interest is the analysis of cerium, a common chemical surrogate for plutonium.^{32–34} Cerium and plutonium have similar chemical and physical properties due to their electronic structures,³⁵ and cerium is often used to gain insight into the behavior of plutonium. In order to be used in nuclear applications, pure plutonium must be alloyed by adding a stabilizing metal to yield its face-centered cubic (FCC) δ phase, rendering it malleable and machineable.^{36–38} Gallium is the most common stabilizer used, but other elements such as aluminium, cerium, silicon, indium and zinc can form a stable or metastable δ state.³⁹ Being able

* Corresponding Author

^a Air Force Institute of Technology, 2950 Hobson Way, WPAFB, OH 45424, USA. E-mail: michael.shattan@afit.edu

^b Actinide Analytical Chemistry, Chemistry Division, Los Alamos National Laboratory, Los Alamos, NM 87545

to rapidly identify and quantify the presence of these dopants at various production stages is critical to ensuring the metal meets chemical and metallurgical specifications.⁴⁰ pLIBS systems assisted by machine learning algorithms could provide a fast, inexpensive, *in-situ* analysis capability to solve this problem.

This study investigates the application of several machine learning techniques to ascertain the superlative approach for spectral analysis of pLIBS data from cerium oxide pellets doped with silicon. We implement an ensemble regression approach, a less common machine learning paradigm in the analytical spectroscopy community, to build predictive models which determine Si content from spectral input. Whereas ensemble methods have been used in LIBS analysis of industrial metals,^{41,42} they have seldom been investigated for radiochemical analysis. These ensemble models are compared to commonly used regression models built using PCA, PLS and ANN methods to evaluate model performance and determine which algorithm provides the most accurate determination of Si content. We organize this paper as follows: sample creation and spectral acquisition methodologies are discussed. Next, simple chemometric regressions using PCA and PLS are presented and evaluated. Two different ensemble regression methods are discussed and their predictive models are analyzed for prediction accuracy. Finally, the ensemble models are compared to an ANN to evaluate their performance against a more common machine learning approach.

2 Experimental

2.1 Sample preparation



Fig. 1 Pellet sample creation equipment used in this study, with inset example of final pellet form. Photo was taken from Wood 2020.⁴³

The ceria pellet samples were prepared from Sigma Aldrich cerium oxide (99.995% CeO₂) mixed with varying weight percent concentrations of silicon dioxide (99% SiO₂). Silicon is a commonly found trace metal impurity in plutonium alloys. Methods developed to discriminate the Si spectral emissions from the bulk Ce emissions could also be applied to other trace metals of interest such as gallium, iron or nickel. The powders were milled using an agate mortar and pestle, weighed to achieve the desired weight percent concentrations and then homogenized using a Fluxana MUK mixer. The mixed powder was then pressed using a 1 cm stainless steel die at 5 metric tons for 120 seconds. 4 different types of ceria samples, doped with 0, 1, 5, and 10 weight percent (wt%) silicon, were created for the experiment. Each sample weighed approximately 1 gram; the mixing and pressing

equipment is shown in Fig. 1.

2.2 Spectral acquisition



Fig. 2 SciAps Z300 LIBS analyzer.²²

A SciAps Z300 hand-held LIBS analyzer (Fig. 2) was used in this study. This device uses a 5-mJ per pulse 1064 nm Nd:YAG laser at a repetition rate of 50 Hz to ablate the surface of a sample, forming a microplasma. Optical emissions from this plasma are collected by the on-board spectrometer system and recorded on a CCD camera, providing a spectral recording from 190-950 nm. The device was used in the gated collection mode, with a delay of 250 ns and fixed integration period of 1 ms. The argon purge feature was used to flush out air from the vicinity of the sample before the data collection shots; an 8x8 raster pattern was used for data collection averaging the spectra of every 16 shots. A total of 176 sample spectra across the four dopant levels, each containing 23431 wavelength variables, were taken for training and testing the developed machine learning algorithms. The raw spectra were normalized using the standard normal variate (SNV) method in Eq. 1; each spectrum (I_k) is centered on its mean value (μ_I) and then divided by the original spectrum standard deviation to yield the SNV normalized spectrum (I_k^{snv}). Normalization is commonly implemented in spectroscopic analysis to reduce signal fluctuation in the raw spectra and yield enhanced analytical performance;⁴⁴ SNV normalization is often implemented in pre-processing LIBS, near-infrared and Raman spectra for this purpose.⁴⁵⁻⁴⁸

$$I_k^{snv} = \frac{I_k - \mu_I}{\sigma_I}, \quad \forall k \quad (1)$$

Normalization was important for this application as the entire spectrum rather than a particular wavelength range was used to train and test the different regression methods. More specifically, SNV was implemented to allow the machine learning models to more easily discriminate the small differences in spectral response among the different sample concentrations. It should be noted that cutting the spectra down and using less wavelength variables could be advantageous, especially since a lot of lighter metals emit at lower wavelengths (200-400 nm), while the higher wavelengths (700+ nm) in the recorded spectra contain mostly emissions from the argon purge gas. However, this initial study sought to test the efficiency of different regression methods with a very complex data set, so all wavelength variables were kept for training and testing.

3 Results

3.1 PCR and PLSR

PCA and PLS represent two different dimensional reduction techniques, often used to simplify analysis of large data sets. Both methods transform raw input data into a smaller set of variables called components, which describe most of the variance of the original data. These components can then be used to analyze the data via visual clustering, or by creating regression models.¹³ PCA is an unsupervised learning method which generates components accounting only for variance in the input data variables, whereas PLS is a supervised learning method that accounts for covariance between the input and output variables in its decomposition. Since PLS attempts to explain covariance structures between input and output variables, it often yields higher accuracy regression models for larger data sets.⁴⁹

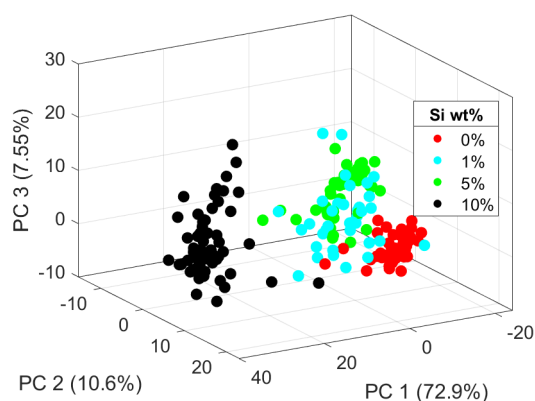


Fig. 3 3D plot of the PC score value of the first three components of each sample. The percent variance of the total data explained in each component is listed on the axis of each PC. The scores plotting reveals overlapping groups of the samples by their Si wt%.

PCA was used to perform an initial analysis of the data to visualize similarities and differences between the samples. Examining a plot of the first three principal component scores which collectively explain greater than 90% of the total spectral variance, displayed in Fig. 3, shows some initial separation between the different sample concentrations. Although a clustering pattern is noticeable, the first three wt% groups show significant overlap. To understand how this could affect a regression model created from the transformed variables, we examine the explained variance of each PC. Typically, PCA is used to reduce the original variable set down to a few principal components representing most of the variance of the original data. The first PC of this deconstruction explains 73% of the total spectral variance. However, examining the first PC loading values of each emission wavelength yields some insight into why the cluster separation is imperfect. The majority of the wavelengths in the first PC with the highest loading values correspond to emissions from the bulk cerium oxide, as seen in Fig. 4. Silicon emissions, often strongest below 400 nm,⁵⁰ load relatively low on this PC despite it explaining the overwhelming majority of the total variance of the entire spectral data set. This indicates that the intensity of the silicon

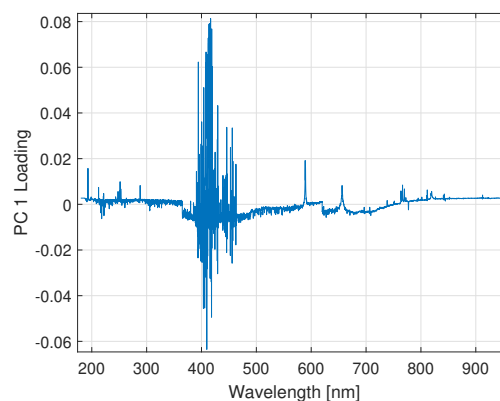


Fig. 4 Wavelength loadings in PC 1. A higher loading value indicates that emission wavelength contributes more to variance of the spectral data set.

emission lines varies significantly less between the different sample concentrations when compared to the cerium emissions. Data corresponding to smaller emissions from the dopants is typically pushed to lower PCs, while higher PCs explain variance of the bulk emissions. As a result of this, a good visual separation between sample types cannot be achieved by simply plotting the scores.

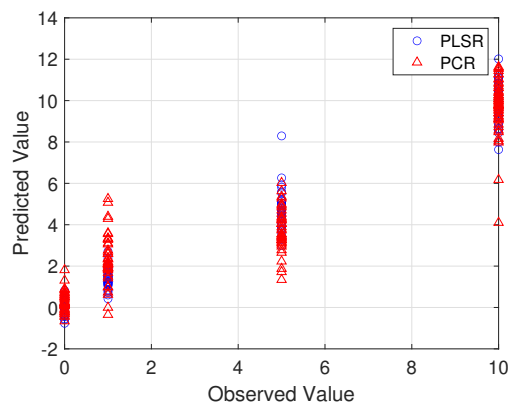


Fig. 5 10-component regression models built with PCA and PLS, comparing the Si content of a sample predicted by the model to the actual value.

This result has significant implications for regressions built from the transformed PC variables. In order to ensure that a regression model can properly distinguish the variations in spectral features between different dopant concentrations, a higher number of components needs to be used in the model. PCs explaining very little of the total variance can often contain important information corresponding to variation in emissions from dopant or impurity elements, and need to be included for accurate determination of elemental concentrations. Ten-component PC regression (PCR) and PLS regression (PLSR) models were built with this data set; the models are compared graphically in Fig. 5, and their R^2 and mean-squared error of prediction ($MSEP$) values are listed in Table 1. The higher R^2 value of the

PLSR model indicates a superior regression fit to the transformed data, whereas the lower *MSEP* indicates a higher predictive accuracy of silicon concentration. As expected, these results indicate that PLSR provides the better regression model.

Table 1 Comparison of R^2 and *MSEP* values for regression models

Model	R^2	<i>MSEP</i>
PCR	0.887	1.926
PLSR	0.967	0.561

3.2 Decision Trees

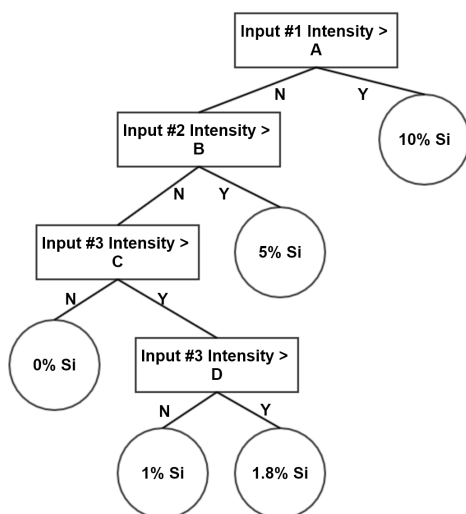


Fig. 6 Example of a lone regression tree for Si content prediction. Each rectangle represents a node, or decision based on the intensity value of a particular emission in the spectra, where A,B,C, and D are values determined by the fit model. Each circle represents a leaf, or outcome, determining the Si content from the flow of the nodes and branches.

Decision trees are a commonly used supervised machine learning technique with applications to a variety of other fields, including data mining, stellar imaging, astrophysics, and molecular modeling.^{49,51–54} Decision trees take input variables and relate them to a target output by following branches across different decision nodes based on the input attribute values, until a terminating node is reached which provides an output result. These algorithms are used in classification and regression, and provide a promising solution to the spectroscopic problem outlined in this study. A graphical depiction of a lone decision tree built from the ceria spectra is shown in Fig. 6, diagramming how the model determines Si content based on the value of different emissions in a spectrum. Whereas a single decision tree model often suffers from overfitting and lower performance with large data sets, an ensemble of trees can improve performance by reducing variance and increasing bias. These types of ensemble methods aim to partition the decision space rather than provide a general separation, making them ideal for use in nonlinear problem spaces. Two ensemble methods, bootstrap-aggregate (also known as bagged) regression trees and boosted ensemble regression trees, were tested

on the LIBS spectra for their ability to predict silicon concentration.

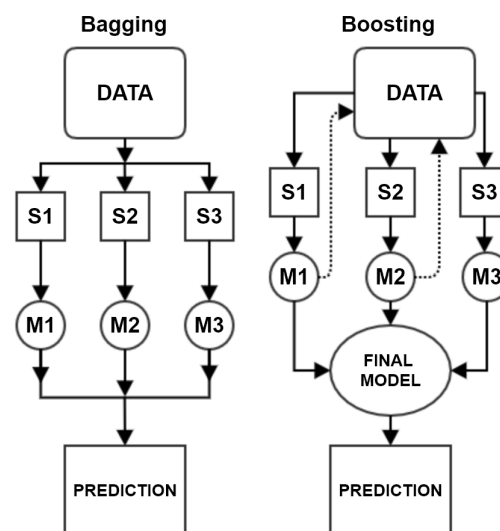


Fig. 7 Comparison of bagging and boosting ensemble methods. Squares denoted by 'S' and 'M' represent data subsets and individual learner models trained on those subsets, respectively.

The methodologies of these ensemble methods are diagrammed in Fig. 7. Bagging uses random replacement sampling to create subsets (S) of the data and independently trains the individual regression models (M), whereas boosting introduces an adaptive algorithm which focuses on areas in the dataset generating higher misclassifications and trains each model sequentially.^{49,51} Whereas bagged models run in parallel and the final prediction is made from an aggregate of each trained model, boosting changes the input weights for each model depending on the error of the previous iteration to improve the accuracy of subsequent learners. Using this sequential adaptive process to mitigate misclassification errors generates improved learners that are combined into a final regression model to make the prediction. The adaptive nature of the boosting algorithm reduces errors in prediction due to variance and bias in the data set, yielding models with significantly lower *MSEPs* and better regression fits. Although both ensemble methods improve model generalization and reduce prediction error, the sequential training process of the boosted ensemble method renders it a "slow learner" compared to the bagged ensemble method, introducing a trade-off between training time and prediction accuracy.⁵⁵

The *TreeBagger* function in MATLAB[®] R2020a was used to construct a bootstrap-aggregated (bagged) regression tree model, using 100 bagged regression trees. The LIBS data was split into a training and testing set using 30% holdout partition. The test data was run through the model using the *predict* function, and a regression, shown in Fig. 8, was calculated between the known test data Si content and the Si content predicted by the model. This bagged regression model gave an R^2 value of 0.974 and an *MSEP* of 0.455, outperforming the PCR and PLSR models discussed in Sect. 2.1 in Si wt% determination. These results clearly indicate that the bagging methodology successfully reduced regression er-

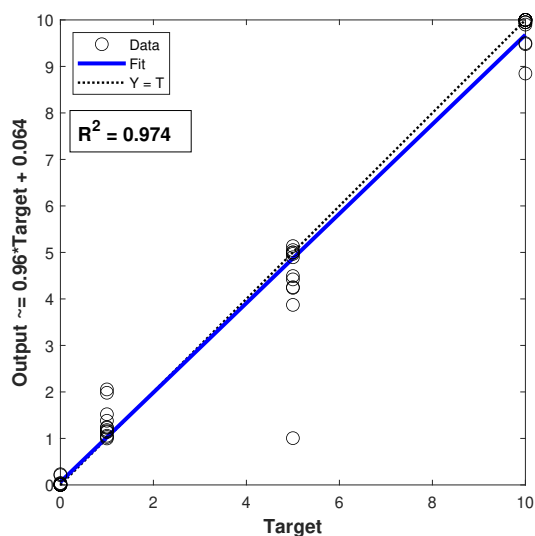


Fig. 8 Bagged ensemble regression model predictions.

ror and improved performance.

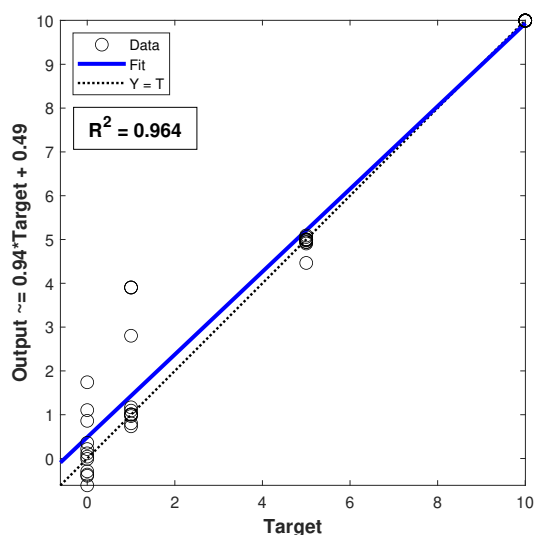


Fig. 9 Boosted ensemble regression model predictions.

The *fitrtree* function in MATLAB[®] R2020a was used to construct a boosted ensemble regression tree model, using 100 boosted trees via a least-squares boosting algorithm. The data was again partitioned using 30% holdout validation. Fig. 9 shows the results of the regression of the predicted Si contents from the boosted ensemble model. The boosted tree regression model yielded a comparable R^2 value (0.964) to the bagged and PLS regression models. However, the *MSEP* for the boosted prediction regression of the test data was driven down to 0.074, an order of magnitude less than the errors of the bagged and PLS regressions. This significant increase in performance indicates that adaptively weighting parts of the input data yielding higher error to train

each learner sequentially resulted in a more accurate final regression model. Bagging falls short in this aspect due to its parallel training method.

It should be noted that while boosting renders a higher accuracy regression, it takes substantially more time to train than the bagged model since it generates and runs all learners in series. The bagged ensemble was trained in 21.67 seconds, whereas the boosted ensemble took 79.01 seconds, nearly four times longer. This highlights the need to consider this trade-off between computational time and accuracy when evaluating which ensemble method to use for a regression solution. In certain cases, especially with limited computational power, it could be advantageous to use a bagged ensemble with less predictive accuracy to enable rapid chemical analysis and quantitative results.

3.3 ANNs

ANNs are a machine learning paradigm inspired by the structure of biological nervous systems. Similar to how a neuron receives input and turns it into a signal to pass to another neuron, a neural network takes a series of input variables and multiplies them by weights. More specifically, data enter an ANN through an input layer and are fed-forward to subsequent layers. Each hidden layer contains neurons (nodes), wherein each neuron sums weighted inputs from the previous layer and generates an output by applying an activation function. The output layer sums weighted inputs from the last hidden layer and generates a numerical output via an activation function.^{49,56} This process is modeled as a mathematical analog of synaptic communication in biological neural pathways; Fig. 10 illustrates a single hidden layer ANN architecture. ANNs have the capability to capture highly complex data

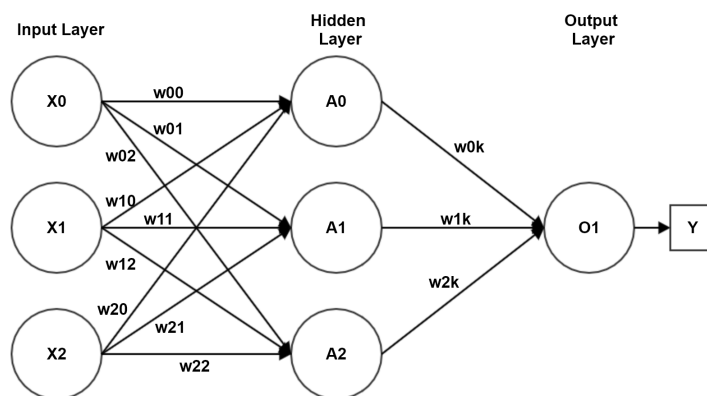


Fig. 10 ANN architecture diagram; each circular node represents a single neuron, and each arrow represents the connection of the output of one neuron to the input of another.

relationships and produce accurate classification or regression solutions for very large data sets, and are often used for image or pattern recognition.^{57,58} Their ability to tie a large number of input variables into a concise output makes them ideal for use in spectroscopy.

The feedforward neural network (FFNN) is a simple, widely used ANN architecture in LIBS analysis.^{18,19,59,60} An FFNN model was created using 15 neurons in the hidden layer; a 70/15/15

percent training/validation/testing partition was applied to the input data, and a scaled conjugate gradient training function was implemented for optimization. The network was run over 42 full learning cycles, or epochs, and its performance is graphically evaluated in Fig. 11. The FFNN produced a model with the lowest

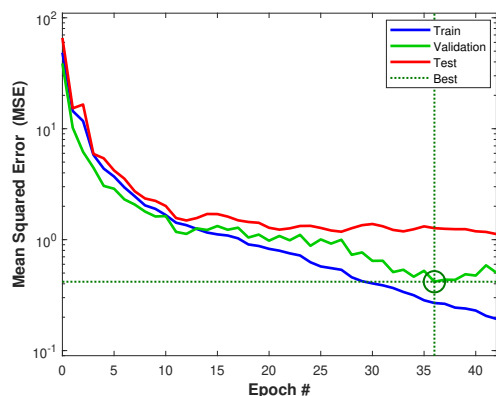


Fig. 11 Feedforward neural network *MSEP* curves over 42 learning cycles.

validation *MSEP* of 0.412, initially indicating high predictive accuracy. Upon closer inspection, however, it appears that this ANN structure suffers from overfitting of the data. In Fig. 11, the training (blue) and validation (green) curves are driven to low *MSEPs*, but the test performance curve (red) has a minimum error almost an order of magnitude higher (1.123) than that of the lowest *MSEP* of the validation curve. This indicates that while the model was able to accurately fit the training data and lower prediction error by updating weights during validation, it failed to generalize these results to the test set. As a result, the FFNN could not provide accurate predictions of Si content for new data. The model can be further analyzed by evaluating the fits of the regressions between the targets and outputs in Fig. 12.

Overall, the FFNN provided good regression fits to the training (Fig. 12a) and validation (Fig. 12b) data, but yielded a poorer fit to the test set ($R^2=0.936$) in Fig. 12c. This yet again indicates overfitting and a failure to properly generalize the model to new data. The model yielded a total R^2 value of 0.975 (Fig. 12d), comparable to the PLSR and ensemble regressions. However, it was outperformed by the boosted ensemble whose *MSEP* remains an order of magnitude lower. Additionally, the boosted regression model was able to properly generalize its training model to the test data, as its R^2 and *MSEP* values from Fig. 9 show high predictive accuracy of new data. Even though both methods provided accurate solutions to this regression problem, the boosted ensemble was able to better generalize the relationship between the spectral inputs and Si content without overfitting the training data during the learning process. Even though ANNs provide a useful tool for relating complex, non-linear input data to a target output, the iterative adaptation of input weights used in the boosted ensemble greatly reduces overall predictive error and yielded a far more robust model in this case.

Although ANNs have traditionally provided accurate regression and classification models for spectroscopic problems, this

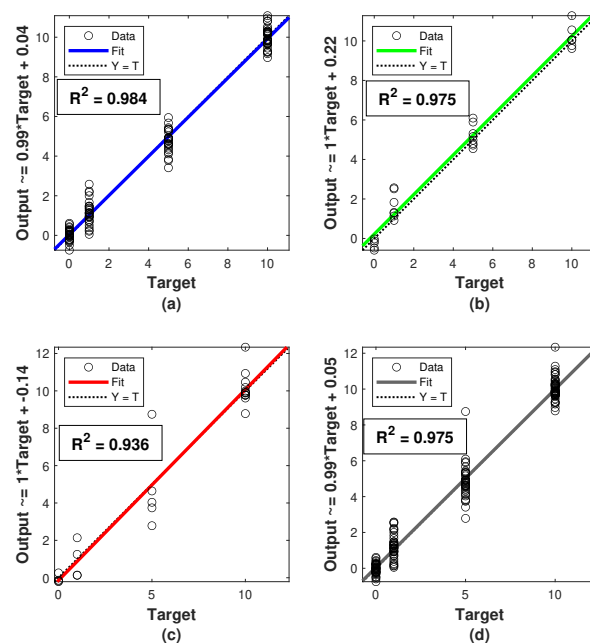


Fig. 12 Feedforward network (a) training, (b) validation, (c) test and (d) total regression fits, with respective R^2 values.

study presents evidence that boosted regression ensembles can be used in-lieu of traditional neural network architectures for rapid and accurate quantification of dopant elements in a bulk cerium matrix. These results are summarized in Table 2, with the best regression performance parameters in boldface. While the bagged ensemble provided the best regression fit ($R^2 = 0.974$), the boosted ensemble yielded an order-of-magnitude improvement in reducing regression error ($MSEP = 0.074$). These results indicate that ensemble methods can provide advantages in accuracy while avoiding overfitting when compared to more common analytical approaches, and present themselves as a promising new tool for use in analytical spectroscopy.

Table 2 Summary of regression model performance parameters

Model	R^2	<i>MSEP</i>
PCR	0.8871	1.926
PLSR	0.967	0.561
Bagged Trees	0.974	0.455
Boosted Trees	0.964	0.074
ANN	0.936	1.123

4 Conclusions

We have reported the evaluation of five machine learning methods to solve a complex chemometric regression problem. LIBS spectra of ceria pellets doped with silicon were used to create predictive models to determine the Si content of a sample from spectral emission information. This study concludes that boosted regression tree ensembles provide better solutions than traditionally used techniques, such as PCR, PLSR and ANN. Boosted en-

semble regressions provided the model with the best fit to the data and highest prediction accuracy based on R^2 and $MSEP$ values. While the ANN model performed well, it displayed evidence of overfitting and could not fully generalize the trained model to make accurate predictions of new input data. This demonstrates the superiority of the boosted ensemble approach in this case. Our results suggest that the boosted ensemble technique may outperform PCAR, PLSR, and ANN approaches for other, similar problems – complex LIBS spectra taken with portable devices. Additional work by the authors will seek to validate this generalization by considering additional sample matrices and additional LIBS instrument variants. Lastly, performance metrics for all tested regression models are tabulated in Table 2.

Conflicts of interest

There are no conflicts to declare.

Acknowledgements

The authors would like to thank the Air Force Office of Scientific Research and the Defense Threat Reduction Agency's Nuclear Technologies Directorate for sponsorship of this research. Additionally this work was reviewed, approved, and released with the LA-UR-20-27109.

Notes and references

- 1 Y. Wu, M. Gragston, Z. Zhang, P. S. Hsu, N. Jiang, A. K. Patnaik, S. Roy and J. R. Gord, *Combustion and Flame*, 2018, **198**, 120 – 129.
- 2 H. Suyanto, N. N. Rupiasih, W. T. B. M. Manurung and K. H. Kurniawan, *AIP Conference Proceedings*, 2012, p. 14.
- 3 D. W. Hahn and N. Omenetto, *Appl. Spectrosc.*, 2012, **66**, 347–419.
- 4 J. L. Gottfried, R. S. Harmon, F. C. D. Lucia and A. W. Miziolek, *Spectrochim Acta B*, 2009, **64**, 1009 – 1019.
- 5 J. Klus, P. Mikysek, D. Prochazka, P. Porizka, P. Prochazková, T. T. J. Novotny and, M. S. K. Novotny and and J. Kaiser, *Spectrochim. Acta B*, 2016, **123**, 143–149.
- 6 P. Porizka, *PhD thesis*, Brno University of Technology, 2014.
- 7 N. Yang, N. Eash, J. Lee, M. Martin, Y.-S. Zhang, F. Walker and J. E. Yang, *Soil Science*, 2010, **175**, 447–452.
- 8 P. Torrione, L. Collins and K. Morton, *Laser Spectroscopy for Sensing*, Woodhead Publishing, 2014, pp. 125 – 164.
- 9 E. Bellou, N. Gyftokostas, D. Stefan, O. Gazeli and S. Couris, *Spectrochimica Acta Part B: Atomic Spectroscopy*, 2020, **163**, 105746.
- 10 P. K. Tiwari, S. Awasthi, R. Kumar, R. K. Anand, P. K. Rai and A. K. Rai, *Lasers in Medical Science*, 2018, **33**, 263–270.
- 11 J. Sirven, A. Pailloux, Y. Baye, N. Coulon, T. Alpettaz and S. Gosse, *J. Anal. At. Spectrom.*, 2009, **24**, 451–459.
- 12 X. Li, Z. Wang, S.-L. Lui, Y. Fu, Z. Li, J. Liu and W. Ni, *Spectrochimica Acta Part B: Atomic Spectroscopy*, 2013, **88**, 180 – 185.
- 13 S. M. Clegg, E. Sklute, M. D. Dyar, J. E. Barefield and R. C. Wiens, *Spectrochimica Acta Part B: Atomic Spectroscopy*, 2009, **64**, 79 – 88.
- 14 R. B. Anderson, J. F. Bell, R. C. Wiens, R. V. Morris and S. M. Clegg, *Spectrochimica Acta Part B: Atomic Spectroscopy*, 2012, **70**, 24 – 32.
- 15 E. D'Andrea, S. Pagnotta, E. Grifoni, G. Lorenzetti, S. Legnaioli, V. Palleschi and B. Lazzarini, *Spectrochimica Acta Part B: Atomic Spectroscopy*, 2014, **99**, 52 – 58.
- 16 V. Motto-Ros, A. Koujelev, G. Osinski and A. Dudelzak, *Journal of the European Optical Society - Rapid publications*, 2008, **3**,.
- 17 T. F. Boucher, M. V. Ozanne, M. L. Carmosino, M. D. Dyar, S. Mahadevan, E. A. Breves, K. H. Lepore and S. M. Clegg, *Spectrochimica Acta Part B: Atomic Spectroscopy*, 2015, **107**, 1 – 10.
- 18 J. El Haddad, M. Villot-Kadri, A. Ismael, G. Gallou, K. Michel, D. Bruyère, V. Laperche, L. Canioni and B. Bousquet, *Spectrochimica Acta Part B: Atomic Spectroscopy*, 2013, **78-79**, 51–57.
- 19 E. C. Ferreira, D. M. Milori, E. J. Ferreira, R. M. Da Silva and L. Martin-Neto, *Spectrochimica Acta Part B: Atomic Spectroscopy*, 2008, **63**, 1216 – 1220.
- 20 Y. Yang, C. Li, S. Liu, H. Min, C. Yan, M. Yang and J. Yu, *Anal. Methods*, 2020, **12**, 1316–1323.
- 21 J. Goujon, A. Giakoumaki, V. Piñon, O. Musset, D. Anglos, E. Georgiou and J. Boquillon, *Spectrochimica Acta Part B: Atomic Spectroscopy*, 2008, **63**, 1091 – 1096.
- 22 SciAps, *SciAps Z Series Spec Sheet*, 2016, https://www.sciaps.com/wp-content/uploads/2016/02/SciAps-Z-Series_Spec-Sheet.pdf.
- 23 R. S. Harmon, R. R. Hark, C. S. Throckmorton, E. C. Rankey, M. A. Wise, A. M. Somers and L. M. Collins, *Geostandards and Geoanalytical Research*, 2017, **41**, 563–584.
- 24 B. Connors, A. Somers and D. Day, *Applied Spectroscopy*, 2016, **70**, 810–815.
- 25 B. T. Manard, M. F. Schappert, E. M. Wylie and G. E. McMath, *Anal. Methods*, 2019, **11**, 752–759.
- 26 R. S. Harmon, F. C. D. Lucia, A. LaPointe and A. W. Miziolek, *Detection and Remediation Technologies for Mines and Mine-like Targets XI*, 2006, pp. 154 – 160.
- 27 B. T. Manard, E. M. Wylie and S. P. Willson, *Applied Spectroscopy*, 2018, **72**, 1653–1660.
- 28 M. B. Shattan, D. J. Miller, M. T. Cook, A. C. Stowe, J. D. Auxier, C. Parigger and H. L. Hall, *Appl. Opt.*, 2017, **56**, 9868–9875.
- 29 A. P. Rao, M. T. Cook, H. L. Hall and M. B. Shattan, *Atoms*, 2019, **7**,.
- 30 A. Rao, *MSc thesis*, Air Force Institute of Technology, 2020.
- 31 A. Rao, J. Auxier, D. Vu and M. Shattan, *Laser Applications to Chemical, Security and Environmental Analysis*, 2020, p. LM1A.2.
- 32 H. Zheng, F.-Y. Yueh, T. Miller, J. Singh, K. E. Zeigler and J. C. Marra, *Spectrochim Acta B*, 2008, **63**, 968–974.
- 33 M. Moore and Y. Tao, *Aerosol Physics Considerations for Using Cerium Oxide CeO₂ as a Surrogate for Plutonium Oxide PuO₂ in Airborne Release Fraction Measurements for Storage Container Investigations*, 2017.

- 34 J. C. Marra, A. D. Cozzi, R. A. Pierce, J. M. Pareizs, A. R. Jurgensen and D. M. Missimer, in *Cerium as a Surrogate in the Plutonium Immobilized Form*, John Wiley & Sons, Ltd, 2012, ch. 36, pp. 381–388.
- 35 F. E. Gibbs, D. L. Olson and W. Hutchinson, *AIP Conference Proceedings*, 2000, **532**, 98–101.
- 36 P. Söderlind, F. Zhou, A. Landa and J. Klepeis, *Scientific Reports*, 2015, **5**, 15958.
- 37 S. S. Hecker, *JOM*, 2003, **55**, 13–19.
- 38 M. Steinzig and F. H. Harlow, *MRS Proceedings*, 1999, **538**,.
- 39 S. S. Hecker, *Plutonium and Its Alloys*, 2000.
- 40 D. Clark, S. Hecker, G. Jarvinen and M. Neu, *Chemistry of the Actinide and Transactinide Elements*, Springer, Dordecht, 2008.
- 41 X. Li, J. Yang, F. Chang, X. Zheng and X. He, *J. Anal. At. Spectrom.*, 2019, **34**, 1135–1144.
- 42 T. Zhang, L. Liang, K. Wang, H. Tang, X. Yang, Y. Duan and H. Li, *J. Anal. At. Spectrom.*, 2014, **29**, 2323–2329.
- 43 J. C. Wood, *MSc thesis*, Air Force Institute of Technology, 2020.
- 44 J. Guezenoc, A. Gallet-Budynek and B. Bousquet, *Spectrochimica Acta Part B: Atomic Spectroscopy*, 2019, **160**, 105688.
- 45 D. Syvilay, N. Wilkie-Chancellier, B. Trichereau, A. Texier, L. Martinez, S. Serfaty and V. Detalle, *Spectrochimica Acta Part B: Atomic Spectroscopy*, 2015, **114**, 38 – 45.
- 46 A. Ismaël, B. Bousquet, K. M.-L. Pierrès, G. Travailé, L. Canioni and S. Roy, *Applied Spectroscopy*, 2011, **65**, 467–473.
- 47 P. Heraud, B. R. Wood, J. Beardall and D. McNaughton, *Journal of Chemometrics*, 2006, **20**, 193–197.
- 48 Y. Guo, Y. Ni and S. Kokot, *Spectrochimica Acta Part A: Molecular and Biomolecular Spectroscopy*, 2016, **153**, 79 – 86.
- 49 D. Larose and C. Larose, *Data Mining and Predictive Analysis*, Wiley, 2015.
- 50 A. Kramida, Y. Ralchenko and J. Reader, *NIST Atomic Spectra Database*, <https://physics.nist.gov/asd>.
- 51 L. Rokach and O. Maimon, *Data Mining with Decision Trees*, World Scientific Publishing Company, 2007.
- 52 L. Rokach and O. Maimon, in *Decision Trees*, ed. O. Maimon and L. Rokach, Springer US, Boston, MA, 2005, pp. 165–192.
- 53 B. Fresch, D. Hiluf, E. Collini, R. D. Levine and F. Remacle, *Proceedings of the National Academy of Sciences*, 2013, **110**, 17183–17188.
- 54 E. Vasconcellos, R. Carvalho, R. Gal, F. LaBarbera, H. Capelato, H. Campos Velho, M. Trevisan and a. Ruiz, *The Astronomical Journal*, 2011, **141**, 189.
- 55 T. Hastie, R. Tibshirani and J. Friedman, *The Elements of Statistical Learning*, Springer-Verlag, New York, 2nd edn, 2009.
- 56 S. Haykin, *Neural Networks: A Comprehensive Foundation*, Prentice Hall, 1999.
- 57 K. J. Cios and I. Shin, *Neurocomputing*, 1995, **7**, 159 – 185.
- 58 W. Mo, X. Luo, Y. Zhong and W. Jiang, *Journal of Physics: Conference Series*, 2019, **1237**, 022026.
- 59 P. Inakollu, T. Philip, A. K. Rai, F.-Y. Yueh and J. P. Singh, *Spectrochimica Acta Part B: Atomic Spectroscopy*, 2009, **64**, 99 – 104.
- 60 A. Koujelev and S.-L. Lui, in *Artificial Neural Networks for Material Identification, Mineralogy and Analytical Geochemistry Based on Laser-Induced Breakdown Spectroscopy*, 2011.